Applied Surface Science 364 (2016) 758–768

Contents lists available at ScienceDirect

Applied Surface Science

journal homepage: www.elsevier.com/locate/apsusc

Insight into the adsorption and dissociation of water over different CuO(111) surfaces: The effect of surface structures

Jin Zhang, Riguang Zhang*, Baojun Wang, Lixia Ling

Key Laboratory of Coal Science and Technology of Ministry of Education and Shanxi Province, Taiyuan University of Technology, Taiyuan 030024, Shanxi, People's Republic of China

ARTICLE INFO

Article history:
Received 1 September 2015
Received in revised form
10 December 2015
Accepted 27 December 2015
Available online 29 December 2015

Keywords:
Water
CuO(111)
Adsorption
Dissociation
Density functional theory

ABSTRACT

Water adsorption and dissociation on solid surfaces play a key role in a variety of industrial processes, a detailed comprehension of this process and the effect of the surface structure will assist in developing the improved catalysts. In this study, the adsorption and dissociation of H_2O on three different types of CuO(111) surfaces, including the stoichiometric, oxygen-vacancy and oxygen-rich surfaces, have been systematically investigated and compared using density functional theory methods. All possible initial configurations of H_2O adsorbed on those surfaces with only one coverage have been identified. Our results show that the adsorption ability of H_2O is substantially weaker than that of the dissociated species (HO, H and O). H_2O chemisorbs at the Cu_{SUB}, Cu^2 and Cu_{SUB} sites of the stoichiometric, oxygen-vacancy and oxygen-rich surfaces, respectively; subsequently, the chemisorption H_2O dissociates into OH and H species. The dissociation mechanisms of chemisorption H_2O and the single OH group leading to the final O and H species suggest that the dissociation of single OH species occurs at a higher barrier compared to the dissociation of OH in the presence of neighboring H atom (produced from the initial step of H_2O dissociation), namely, the presence of H is in favor of OH dissociation, which agrees with the results of charge transfer. However, owing to the significantly high barrier of OH dissociation compared to the initial dissociation step of H_2O, OH species is considered as the dominant product on those surfaces. Oxygen-rich surface is the most favorable for the initial dissociation of H_2O both thermodynamically and kinetically than other two surfaces. The calculated vibrational frequencies for the adsorbed H_2O and OH species on CuO(111) surfaces can be applied to guide the experimental research of surface vibrational spectroscopy. In addition, our results may provide a basis for the study of H_2O interaction with other metal oxide surfaces.

1. Introduction

The interaction of water (H_2O) with solid surfaces has drawn a considerable attention because of its fundamental importance in various different fields of science [1–10]. Plenty of catalytic reactions involve H_2O as a reactant or product, including the Fischer–Tropsch synthesis, dimethyl carbonate synthesis via oxidative carbonylation of methanol, and so on. Over the past decades, many experimental and theoretical investigations have been devoted to the adsorption of H_2O on the surfaces of metal catalyst such as Ni(111) [11], Rh(111) [12], Au(111) [13], Ag(100) [14] and Pd(111) surfaces [15], and so on. Compared to above metals, Cu has been widely used due to its low cost and the relatively high activity toward H_2O dissociation into OH and H species [16]. However, the active center of Cu has been a matter of debate in the literature for the past twenty years [17–20], for example, the studies by Shefer and King [17], Herman et al. [18], Zuo et al. [21] have proposed that Cu_2O presents the higher catalytic activity for the synthesis of methanol from CO/H_2 compared to Cu, moreover, copper-oxygen systems have been investigated extensively in order to make out the reactivity and electronic nature of H_2O on the surface [22].

Up to now, the interaction of hydrogen, oxygen, water, alcohols and hydrogen sulfide with Cu_2O surfaces have been widely investigated [23–29]. In the case of water, Saraire et al. [25] have carried out a theoretical simulation of H_2O adsorption and dissociation on $Cu_2O(110)$ surface, suggesting that the molecular adsorption of H_2O is most likely to be preferred over dissociative adsorption according to the extremely high activation energies for the formation of dissociative moieties. Zhang et al. [26] and Li et al. [27] have systematically investigated the adsorption and dissociation of H_2O

* Corresponding author at: No. 79 Yingze West Street, Taiyuan 030024, People's Republic of China.
E-mail addresses: zhangriguang@tyut.edu.cn, zhangriguang1981@163.com (R. Zhang).

http://dx.doi.org/10.1016/j.apsusc.2015.12.211
0169-4332/

on $Cu_2O(111)$ and $Cu_2O(100)$ using density functional theory (DFT) calculations, respectively. On the other hand, Wang et al. [30] have experimentally investigated a new type of supported oxide catalyst CuO–La_2O_3/activate carbon (AC), which simultaneously contained CuO and Cu_2O. Then, the experimental results from Zhang et al. [31] have shown that the CuO/AC catalyst presents a good catalytic activity for the oxidative carbonylation of methanol. Up to now, to the best of our knowledge, few studies have been systematically reported for the adsorption and dissociation of H_2O on CuO surface, especially for the CuO(111) surface, which is the most stable surface of CuO [32], only Hu et al. [33] have investigated the adsorption of H_2O on the stoichiometric CuO(111) surface using DFT methods. Meanwhile, previous studies in the copper oxide atomic layer deposition from $Cu(acac)_2$ (acac = acetylacetonate) have reported the reaction between H_2O and $Cu(acac)_2$ on the stoichiometric CuO(111) surface [34]. Maimaiti et al. [35] have explored the reduction mechanisms by oxygen vacancy formation on CuO(111) surface, suggesting that the surface O_{SUF} atom is pulled out from the surface upon interaction with H_2 to form a H_2O molecule, which ultimately adsorbed at the surface Cu site on the oxygen-vacancy surface. However, the adsorption behavior and dissociation mechanisms of H_2O on the stoichiometric and oxygen-vacancy CuO surface are still unclear at present. Consequently, it is necessary to explore the adsorption and dissociation of H_2O on different types of CuO(111) surfaces.

Actually, the metal oxide surfaces are not always stoichiometric under a realistic condition, and the presence of surface oxygen-vacancies plays an important role in surface reactivity, as well as many other important properties of metal oxides [36]. For example, the presence of oxygen-vacancies over $Cu_2O(111)$ surface leads to the dissociative adsorption of H_2O, and has a lower energy barrier of the O—H bond cleavage for the molecular adsorption H_2O compared to the stoichiometric $Cu_2O(111)$ surface [26]. Recent studies by DFT calculations have observed that the oxygen-vacancy on CuO(111) surface could be of great significance toward the catalytic reactivity of O_2 adsorption and dissociation, and the presence of oxygen-vacancy can contribute to the lower activation barrier for O_2 dissociation than that on the stoichiometric surface [37]. On the other hand, the effect of surface modification by oxygen-rich atoms on CH_3OH activation has been investigated on several metal electrodes [38–42], Cu_2O [29] and CuCl [43] surfaces, indicating that the surface oxygen-rich atom can change the dissociation barrier of O—H bond. The dissociation mechanisms of CH_3OH to form CH_3O on the oxygen-rich CuO(111) surface have suggested that the oxygen-rich atom plays an important role in CH_3O formation [44]. Yet, up to now, few studies about the O—H bond activation of H_2O on the oxygen-rich CuO(111) surface have been reported.

As mentioned above, DFT calculations have been used as a powerful tool to investigate the adsorption and dissociation of H_2O on Cu_2O surfaces, which can be helpful to clarify the underlying mechanism at a molecular level [25–27]. As a result, by means of DFT calculations, a specific investigation of H_2O adsorption and dissociation on different CuO(111) surfaces will also help us fully understand the underlying mechanisms of H_2O interaction with CuO(111) surface at a molecular level.

In this work, by means of the first-principles DFT calculations, the adsorption site of H_2O and its dehydrogenation on the stoichiometric, oxygen-vacancy and oxygen-rich CuO(111) surfaces have been systematically investigated to illustrate the mechanism of H_2O dissociation. Firstly, the adsorption energies and the stable adsorption geometries of molecular H_2O, as well as its dissociation products on different CuO(111) surfaces have been examined. Then, the energetics of the involved elementary reactions is analyzed including the thermochemistry and relevant barriers for H_2O dissociation on these surfaces. Further, we discuss the effect of CuO(111) surface structures on H_2O adsorption and dissociation.

2. Computational models and methods

2.1. Surface models

The unit cell of CuO is that each atom has four nearest neighbors of another species, oxygen atom is surrounded by a distorted tetrahedron of copper atoms while each Cu atom is surrounded by a square of oxygen atoms [45,46]. CuO(111) surface has been widely chosen as an ideal model system to investigate the structure, stability and adsorption properties, since it is the most stable surface of CuO under the realistic catalytic conditions [37,44,47].

As an important crystal face, CuO(111) surface is modeled by using the supercell approach, where the periodic boundary condition is applied to the central supercell so that it is reproduced periodically throughout space. Fig. 1(a) displays the side view and top view of stoichiometric CuO(111) surface. The stoichiometric CuO(111) surface includes eight types of surface adsorption sites: Cu_{SUF}, Cu_{SUB}, O_{SUF}, O_{SUB}, Cu_{SUB}–Cu_{SUB} bridge, O_{SUB}–O_{SUB} bridge, O_{SUF}–O_{SUF} bridge and Cu_{SUF}–Cu_{SUF} bridge sites, which are named as I, II, III, IV, V, VI, VII and VIII, respectively. Cu_{SUF}(I) site is the outer-most surface copper atom, and Cu_{SUB} (II) site is the subsurface copper atom. O_{SUF} (III) site is the outer-most surface oxygen atom, and O_{SUB} (IV) site is the subsurface oxygen atom [47]. Moreover, the oxygen-vacancy CuO(111) surface is derived from the removal of outer-most surface oxygen atom from the stoichiometric CuO(111) surface [37], as shown in Fig. 1(b). Each oxygen vacancy generates a three-fold site of Cu^+ cation (i.e., Cu^2, Cu^3 and Cu^4 atoms).

Different CuO(111) surfaces are modeled using a $p(3 \times 2)$ unit cells with six atomic layers. The top three atomic layers of the substrate and the adsorbed species are relaxed while the bottom three layers of the substrate are kept fixed to maintain the bulk crystal structure. A vacuum layer of 10 Å along the z-direction perpendicular to the surface is employed, which is enough to eliminate the spurious interactions between the adsorbate and the periodic image of the bottom layer of the surface repeated slabs.

2.2. Calculation methods

All density functional theory (DFT) calculations are performed with $Dmol^3$ program package in Materials Studio 8.0 [48,49]. In the computation, the generalized gradient approximation (GGA) functional developed by Perdew and Wang (PW91) has been employed [50–52]. The inner electrons of copper atoms are kept frozen and substituted by a DFT Semi-core Pseudopots (DSPP), and other atoms are treated with an all-electron basis set. The valence electrons functions are expanded into a set of numerical atomic orbitals by a double-numerical basis with polarization functions (DNP) [53,54]. Brillouin-zone integrations have been performed using $3 \times 3 \times 1$ Monkhorst-Pack grid and a Methfessel-Paxton smearing of 0.005 Ha [37]. Spin unrestricted has been considered. All the energetics obtained in our calculation are computed at $T = 0$ K.

For the purpose of determining accurate activation barriers of H_2O dissociation, we select complete LST/QST approach to search for the transition states of dissociation reactions [55], starting from the reactants and products, the LST (linear synchronous transit) method performs a single interpolation to a maximum energy, and the QST (quadratic synchronous transit) method alternates searches for an energy maximum with constrained minimizations in order to refine the transition state to a high degree. In addition, a vibrational frequency analysis has been calculated to validate the true nature of the saddle point by identifying only a single imaginary frequency along the reaction coordinate, and Transition state (TS) confirmation is performed on every transition state to confirm that they lead to the desired reactants and products.

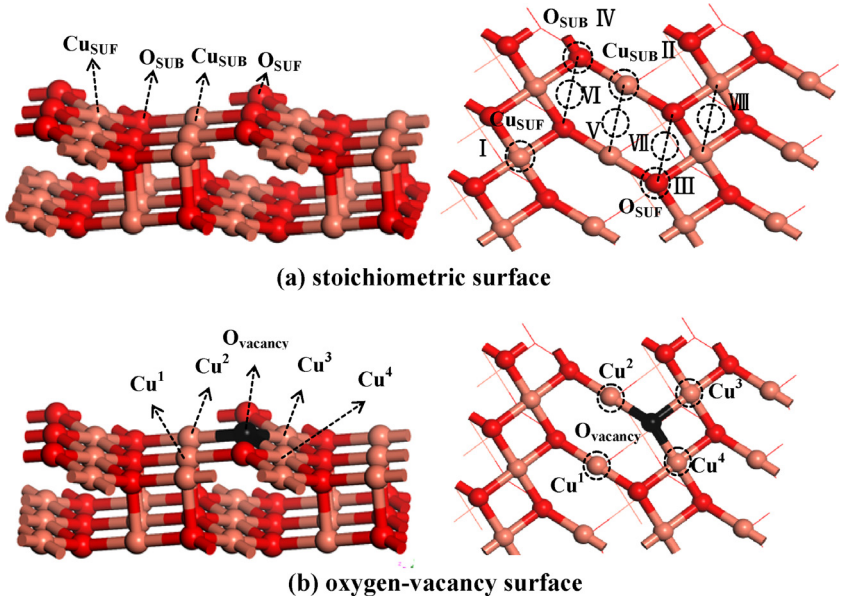

Fig. 1. The slab models of a $p(3 \times 2)$ CuO(111) surface. Orange, red and black balls stand for Cu, O atoms and the oxygen-vacancy site, respectively. (For interpretation of the references to color in this figure legend, the reader is referred to the web version of the article.)

The reaction energy (ΔE) and the activation barrier (E_a) are defined as follows:

$$\Delta E = E_P - E_R$$

$$E_a = E_{TS} - E_R$$

where E_R and E_P are the energies of the reactant and product in each elementary reaction, respectively, and E_{TS} is the energy of the transition state in each elementary reaction.

3. Results and discussion

3.1. Evaluation of the method and model

In order to validate the reliability of the computational method and model, we calculate the angle of H—O—H, as well as the bond length for O—H of H_2O in gas phase, which are 103.9° and 0.970 Å, respectively, which agree well with the experimental values of 104.5° and 0.957 Å, respectively [56]. Then, the bulk lattice parameters of CuO are tested. CuO has a monoclinic structure with the space group C2/c1 (a = 4.684 Å, b = 3.423 Å, c = 5.129 Å and β = 99.54°) [57]. The calculated lattice constants of bulk CuO are a = 4.653 Å, b = 3.410 Å, c = 5.108 Å and β = 99.50°. Above results obtained in these tests make us confident in the chosen method and model in order to describe the features of the potential energy surface for H_2O adsorption and dissociation on CuO(111) surface.

3.2. Adsorption of OH and atomic O, H species on CuO(111) surface

The adsorption energy is always regarded as a measure of the strength of adsorbate–substrate adsorption. The adsorption energy can be defined as the following equation:

$$E_{ads} = E_{sub} + E_{mol} - E_{mol/sub}$$

where E_{ads} is the adsorption energy, $E_{mol/sub}$ is the total energy of adsorbate–substrate system in its equilibrium state, E_{sub} is the energy of the substrate, and E_{mol} is the energy of the isolated adsorbate. By means of this definition, a higher positive value of E_{ads} corresponds to a stronger adsorption.

In this section, the adsorption of OH, atomic O and H on CuO(111) surface have been investigated in detail, which is at a coverage of 1/6 ML with one absorbed species in a $p(3 \times 2)$ unit cell. Eight different adsorption sites presented in Fig. 1(a) have been examined on the stoichiometric CuO(111) surface, while $O_{vacancy}$ site is employed on the oxygen-vacancy surface, as shown in Fig. 1(b).

3.2.1. Atomic H adsorption

In the case of atomic H adsorbed on the stoichiometric CuO(111) surface, six stable adsorption configurations obtained after optimization, as shown in Fig. 2(a)–(f), in which H initially lies over Cu_{SUF}–Cu_{SUF} and O_{SUF}–O_{SUF} bridge sites, H transfers to O_{SUF} site after optimization. In the case of $O_{vacancy}$ site, H is optimized to the Cu^2-Cu^3 bridge site, as shown in Fig. 2(c), which is different from that on the oxygen-vacancy Cu_2O(111) surface that H is adsorbed at the $O_{vacancy}$ site [23]. The adsorption energy of H adsorption at different adsorption sites of CuO(111) surface are presented in Table 1, which could be assigned in the following order: $H(O_{SUF}) > H(O_{SUB}) > H(Cu^2–Cu^3) > H(Cu_{SUB}–Cu_{SUB}) > H(Cu_{SUB}) > H(Cu_{SUF})$, indicating that O_{SUF} site is the most stable site for H adsorption on CuO(111) surface.

3.2.2. Atomic O adsorption

For atomic O adsorption on CuO(111) surface, the initial configurations at nine different adsorption sites are considered. After optimization, we can only obtain three stable adsorption configurations, as presented in Figs. 2(g)–(i). For the stoichiometric surface, atomic O is adsorbed at the Cu_{SUB}-Cu_{SUB} bridge and Cu_{SUB} sites, respectively. While in the case of the oxygen-vacancy surface, the vacancy site is filled with O atom.

As listed in Table 1, the adsorption energies of these three stable configurations are in the following order: $O(O_{vacancy}) > O(Cu_{SUB}–Cu_{SUB}) > O(Cu_{SUB})$, suggesting that O atom bonds with two Cu_{SUB} atoms via the bridge mode is the most favorable configuration on the stoichiometric surface, while $O_{vacancy}$ site is the active center for atomic O adsorption on the oxygen-vacancy surface.

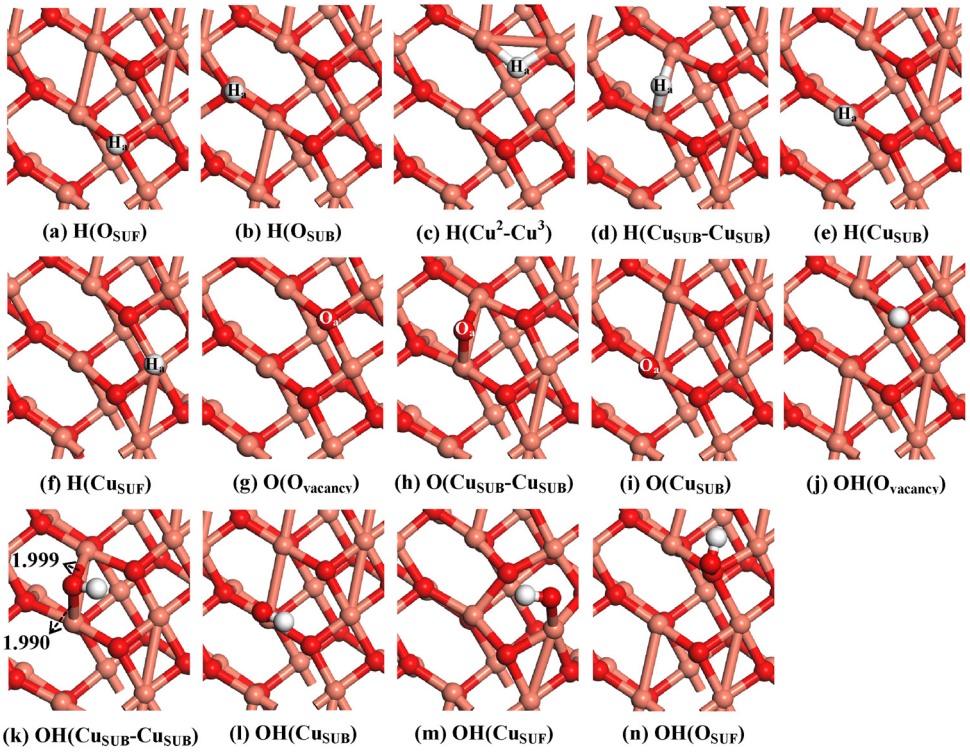

Fig. 2. Optimized adsorption configurations of H, O and OH species on CuO(111) surface. White balls stand for H atoms, and others are the same as in Fig. 1. Bond lengths are in Å.

3.2.3. OH adsorption

Two molecular orientations for OH adsorption, O-down and H-down, over nine adsorption sites of CuO(111) surface are considered. The O—H axis is perpendicular to the surface in all the optimized models. For the H-down modes, it is interesting to find that all H-down models are all converted to the O-down modes after optimization.

In the case of O-down molecular orientation, we obtain five stable adsorption configurations, as shown in Figs. 2(j)–(n). The corresponding adsorption energy are shown in Table 1, we clearly find that the structure of OH($O_{vacancy}$) has the largest adsorption energy (410.1 kJ mol^{-1}) compared to other four configurations, in which $O_{vacancy}$ site is filled with OH via O atom, the H—O bond length is 0.976 Å. The bands at 3677 and 819 cm^{-1} are observed, which correspond to the O—H stretching and Cu—O—H bending modes of adsorbed OH species. For the stoichiometric surface, Cu_{SUB}–Cu_{SUB} bridge site is the active center for OH group adsorption, the corresponding adsorption energy is 254.8 kJ mol^{-1}, as shown in Fig. 2(k), the distances of Cu_{SUB}–O are 1.999 and 1.990 Å, respectively, the bands appear at 3661 and 786 cm^{-1} are attributable to the O—H stretching and Cu—O—H bending modes of adsorbed OH species. Therefore, OH adsorption with O-down mode at the Cu_{SUB}–Cu_{SUB} bridge and $O_{vacancy}$ sites are the most stable configurations on the stoichiometric and oxygen-vacancy CuO(111) surfaces, respectively.

On the other hand, partial density of states (PDOS) can provide fundamental understanding about the interactions of the adsorbate–substrate [58]. Fig. 3 presents the PDOS for the orbitals of O atom in the adsorbed OH at the Cu_{SUB}–Cu_{SUB} bridge site and for the vicinal Cu atoms on the stoichiometric surface. For the orbital contribution of O atom in OH, from −19.8 to −17.1 eV, the total DOS is mainly contributed by O 2s orbital; while in other energy regions, the total DOS are predominantly contributed by O 2p orbital. Meanwhile, for the orbital contribution of Cu atom, from −7.29 to 1.37 eV, Cu 3d orbital dominantly contributes to the total DOS. A slight peak is observed nearby −19.1 eV, which comes from the hybridization between O 2s orbital and Cu 3d (4s) orbital. Further, as shown in Fig. 3(c), the interactions between Cu 3d and O 2p states are quite strong at the energy level around −6.71, −3.81, −2.22, and −0.07 eV, respectively.

Table 1
The adsorption energies (E_{ads}) of H, O and OH species for the stable adsorption configurations at different sites on CuO(111) surface presented in Fig.2.

Model	E_{ads} (kJ mol^{-1})	Model	E_{ads} (kJ mol^{-1})
H(O_{SUF})	333.4	O(Cu_{SUB}–Cu_{SUB})	272.1
H(O_{SUB})	314.7	O(Cu_{SUB})	215.5
H(Cu^2–Cu^3)	272.7	OH($O_{vacancy}$)	410.1
H(Cu_{SUB}–Cu_{SUB})	194.4	OH(Cu_{SUB}–Cu_{SUB})	254.8
H(Cu_{SUB})	182.3	OH(Cu_{SUB})	231.6
H(Cu_{SUF})	92.9	OH(Cu_{SUF})	130.6
O($O_{vacancy}$)	551.1	OH(O_{SUF})	82.9

3.3. Adsorption and dissociation of H_2O on the stoichiometric surface

3.3.1. H_2O adsorption

For H_2O adsorption on the stoichiometric surface, two types of initial configurations have been considered, one is that H_2O is perpendicular to the surface with O binding to the adsorption sites; the other is that H_2O is parallel to the surface with O binding to the adsorption sites.

After optimization, we interestingly find that the adsorption energies for most of the stable configurations are about 40 kJ mol^{-1}, and only two adsorption energies are above 80 kJ mol^{-1}, as shown in H_2O(1) and H_2O(IS1) of Fig. 4. For these two structures, H_2O is adsorbed at the Cu_{SUB} site via atomic O. Meanwhile, in H_2O(1) model, one H atom points to O_{SUF} site and another H atom is inclined to adsorb at O_{SUB} site; in H_2O(IS1) model, two H atoms completely point toward two O_{SUF} sites. The adsorption energies of H_2O(1)

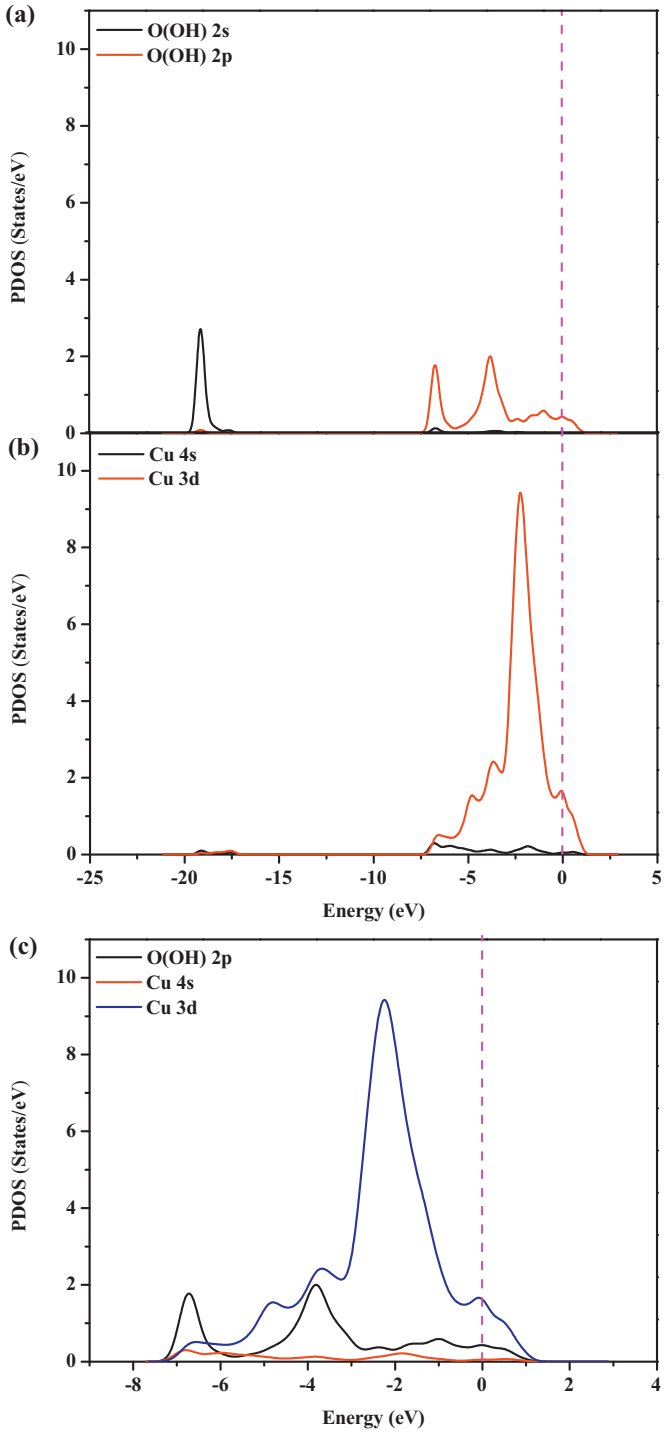

Fig. 3. Partial density of states (PDOS) of (a) O atom in the adsorbed OH at the Cu_{SUB}–Cu_{SUB} bridge site, (b) the vicinal Cu atoms, and (c) the enlarged view from −8.00 to 2.00 eV on the stoichiometric surface (vertical dotted line denoted as the fermi level).

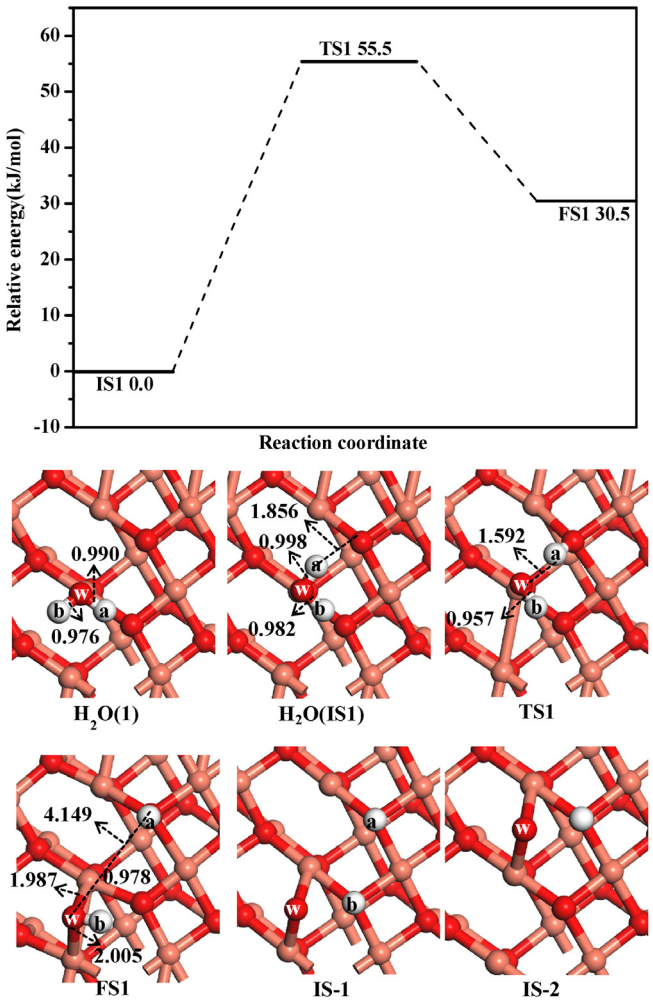

Fig. 4. Two optimized stable configurations of H_2O species adsorbed at Cu_{SUB} site, and the potential energy profiles for the dehydrogenation of chemisorption H_2O at Cu_{SUB} site together with the initial states (IS1), transition states (TS1) and final states (FS1), as well as the initial co-adsorption structures of H + O + H (IS-1) and O + H (IS-2) on the stoichiometric CuO(111) surface. Bond lengths are in Å. See Figs. 1 and 2 for color coding.

and H_2O(IS1) are 80.4 and 87.0 kJ mol^{-1}, respectively. Thus, in the combination with above result that O_{SUF} is the active center for H adsorption, H_2O(IS1) is considered as the most favorable adsorption configuration.

In H_2O(IS1) structure, one Cu_{SUB}—O bond (2.124 Å) is formed, and the H_a—O bond of H_2O (0.998 Å) is stretched relative to that in free H_2O molecule (0.970 Å), which can contribute the activation and dissociation of H_2O. Our calculated bands for H_2O adsorbed at Cu_{SUB} site appear at 3636 and 3232 cm^{-1} due to the anti-symmetric and symmetric O—H stretching vibrations of H_2O, respectively, and 1640 cm^{-1} is contributed to the H—O—H bending modes. Moreover, our bands in the free H_2O molecule are seen at 3854 and 3735 cm^{-1} due to the anti-symmetric and symmetric O—H stretching vibrations, as well as that at 1629 cm^{-1} for the H—O—H bending modes. Compared to the free H_2O molecule, the red-shift of the O—H stretching vibration frequency for the adsorbed H_2O indicates that the strength of H—O bond decreases, which agrees with the results obtained from the O—H bond length of the adsorbed H_2O.

3.3.2. H_2O dissociation

For H_2O dissociation on the stoichiometric surface, we firstly focus on the dissociation mechanism of chemisorption H_2O. The dissociation mechanism involves the sequential dehydrogenation of H_2O. This sequential O—H dissociation give rise to OH, O and H species over the surface (i.e. the first step is that $H_2O_{(ads)} \rightarrow H_{(ads)} + OH_{(ads)}$, and the second step is that $OH_{(ads)} \rightarrow H_{(ads)} + O_{(ads)}$). Then, the thermochemistry, activation barrier of each elementary step, as well as its dissociation products have been systematically discussed.

As shown in Fig. 4, the most stable adsorption configuration H_2O(IS1) is chosen as the initial state for our research in the first dissociation reaction of H_2O on the stoichiometric surface. The

resulting intermediates of O_w—H_a scission in H_2O are H_a and O_wH_b. As mentioned above, the Cu_{SUB}—Cu_{SUB} bridge site is the favorable sites for OH adsorption with O-down mode, and H atom is adsorbed preferentially at the O_{SUF} site. Therefore, the initial co-adsorption configuration is that H_a and O_wH_b are adsorbed at the O_{SUF} and Cu_{SUB}—Cu_{SUB} bridge site, respectively, the optimized configuration is regarded as the final state (FS1) for the first dehydrogenation of H_2O.

Fig. 4 presents the potential energy profiles for H_2O dissociation together with initial states (IS1), transition states (TS1), final states (FS1), we can see that in TS1, H_2O breaks one H_a—O_w bond by tilting one H_a atom toward a nearby surface O_{SUF} atom, and the H_b—O_w bond adsorbed at the Cu_{SUB} site, this reaction is endothermic by 30.5 kJ mol^{-1} with an activation barrier of 55.5 kJ mol^{-1}. The dissociating O_w—H_a bond distance is about 1.592 Å, which is longer by 0.594 Å than that in IS1 (0.998 Å). The O_w—Cu_{SUB} bond length is 1.921 Å, which is smaller by 0.203 Å than that in IS1 (2.124 Å). In FS1, the O_wH_b group is aslant adsorbed at the Cu_{SUB}–Cu_{SUB} site with the O_w—Cu_{CUB} bond lengths of 1.987 and 2.005 Å, respectively, which are smaller by 0.137 and 0.119 Å than those in IS1, respectively.

3.3.3. OH dissociation

To characterize OH dissociation on the stoichiometric CuO(111) surface, FS1 is selected as the initial state of OH dissociation in the second dissociation step of H_2O. As for the final state, we firstly choose the initial co-adsorption configuration of one O_w and two H atoms, which are adsorbed at the Cu_{SUB}–Cu_{SUB} bridge and two adjacent O_{SUF} sites, respectively, as shown in Fig. 4(IS-1). However, the optimized configuration is converted to FS1, namely, the co-adsorption configuration of one O_w and two H atoms cannot exist.

On the other hand, in order to gain insight into the H—O bond-breaking process, we also examine the dissociation of the single OH group adsorbed on the stoichiometric surface, as mentioned in Fig. 2(k), the single OH group with O-down adsorbed at Cu_{SUB}–Cu_{SUB} bridge is chosen as the initial state. The final state is the co-adsorption of O and H atoms located at the Cu_{SUB}–Cu_{SUB} bridge and O_{SUF} sites, respectively, as shown in Fig. 4(IS-2), however our results show that the optimized configuration is converted to the structure shown in Fig. 2(k), namely, the co-adsorption configuration of O and H atoms also cannot stably exist.

Therefore, we clearly draw a conclusion that OH, not only from the first dissociation step of H_2O, but also the single OH group, is failed to dissociate on the stoichiometric surface.

3.3.4. Brief summary

From Fig. 4, we can clearly see that the first dehydrogenation step of H_2O needs to overcome an activation barrier of 55.5 kJ mol^{-1}, which is lower than the adsorption energy (87.0 kJ mol^{-1}) of chemisorption H_2O on the stoichiometric surface, namely, the chemisorption H_2O prefers to dissociate into OH and H species rather than desorption; while OH group from the first dehydrogenation step of H_2O or the single OH group failed to be dissociated into O and H species, suggesting that OH and H species are the most favorable products of H_2O dissociation on the stoichiometric CuO(111) surface.

3.4. Adsorption and dissociation of H_2O on the oxygen-vacancy surface

As we all know, a majority of reactions on catalytic surface significantly influenced by the surface defects [59–61]. In this section, we choose oxygen-vacancy surface to model H_2O adsorption and dissociation on the defective surface. The adsorption of H_2O on the oxygen-vacancy CuO(111) surface is at a coverage of 1/6 ML with one molecule in every (3×2) unit cell. Obviously, the geometric structures of $p(3 \times 2)$ with 17% oxygen-vacancies (1/6 of O_{SUF} atoms are missing) are a great deal of vacancies, which may not exist under the realistic reaction condition. However, the intention in this study is to obtain only a sufficient qualitative understanding about the effect of oxygen-vacancy surface on H_2O adsorption and dissociation. As mentioned above, the oxygen-vacancy surface exhibits three kinds of catalytic active sites subjected to the adsorption of H_2O: Cu^1, Cu^2 and $O_{vacancy}$ sites. The Cu atoms nearby the $O_{vacancy}$ site are Cu^1, Cu^2, Cu^3 and Cu^4 atoms remarked in Fig. 1(b). Among the four Cu atoms, Cu^1 and Cu^2 are the doubly and singly coordinated, respectively, while Cu^3 and Cu^4 belong to the same kind with the triple coordination.

3.4.1. H_2O adsorption

Regarding the adsorption of H_2O on the oxygen-vacancy surface, as shown in Fig. 5(a)–(h), eight types of original adsorption configurations have been taken into considerations, denoted as IC-x, (1) H_2O lies over Cu^1 site with O atom in a V-shape structure; (2) H_2O lies over Cu^2 site with O atom in a V-shape structure; (3) H_2O lies over $O_{vacancy}$ site with O atom in a V-shape structure; (4) H_2O lies over Cu^1–$O_{vacancy}$ bridge site with O atom in a V-shape structure; (5) H_2O lies over Cu^1–Cu^2 bridge site with O atom in a V-shape structure; (6) H_2O lies over Cu^2–Cu^4 bridge site with O atom in a V-shape structure; (7) H_2O lies over $O_{vacancy}$ site via O and H atoms in η^2–O–η^1–H configuration of L-shape; (8) H_2O lies flatly over Cu^1–$O_{vacancy}$ bridge site O and H atoms in η^2–O–η^1–H configuration of L-shape. Figs. 5(i) and (j) also present the optimized configurations of above initial adsorption configurations.

Our results indicate that except for IC-1 mode, all other initial adsorption configurations are all converted to the optimized OS-1 structure. In OS-1 structure, H_2O is adsorbed at the Cu^2 site, the H_a—O bond of H_2O (1.014 Å) is significantly stretched relative to that in free H_2O molecule (0.970 Å), which can contribute to the dehydrogenation of H_2O. In addition, the plane of H_2O molecule is nearly parallel to the surface and the corresponding adsorption energy is 124.4 kJ mol^{-1}. Our vibration frequencies for adsorbed H_2O show that the bands appear at 3718 and 2944 cm^{-1} due to the anti-symmetric and symmetric O—H stretching vibrations of H_2O, and 1576 cm^{-1} is contributed to the H—O—H bending modes. Similar to the stoichiometric surface, the red-shift of the O—H stretching frequencies indicates that the strength of O—H bond decreases, which is in line with the results obtained from the O—H bond length. On the other hand, the initial adsorption structures of IC-1 is converted to OS-2 configuration after optimization, the O—H bond lengths are 0.976 and 0.875 Å, respectively, where one O—H bond is almost unchanged and the other is shorter compared to that in the free H_2O molecule (0.970 Å), the corresponding adsorption energy is 106.8 kJ mol^{-1}.

The adsorption energies of above two structures are in the following order: OS-1 > OS-2, suggesting that Cu^2 site with the singly coordinate is the most stable site for H_2O adsorption on the oxygen-vacancy CuO(111) surface.

3.4.2. H_2O dissociation

Different from the previous work by Zhang et al. [26] that H_2O dissociative adsorption on the oxygen-vacancy Cu_2O(111) surface is the main pathway, chemisorption H_2O at the Cu^2 site is the only initial dissociation way on the oxygen-vacancy CuO(111) surface. Consequently, the structure OS-1 shown in Fig. 5 is chosen as the initial state (IS2) and the co-adsorption configuration of OH and H species is selected as the final state (FS2) to probe into the first dissociation step of H_2O on the oxygen-vacancy CuO(111) surface.

The potential energy profiles of H_2O dissociation on the oxygen-vacancy surface as well as the corresponding structures are shown in Fig. 6. The initial structure (IS2) can form the co-adsorbed O_wH_b and H_a species (FS2) via a transition state TS2. Namely, H_2O is initially adsorbed at the Cu^2 sites with the O_w—H_a bond

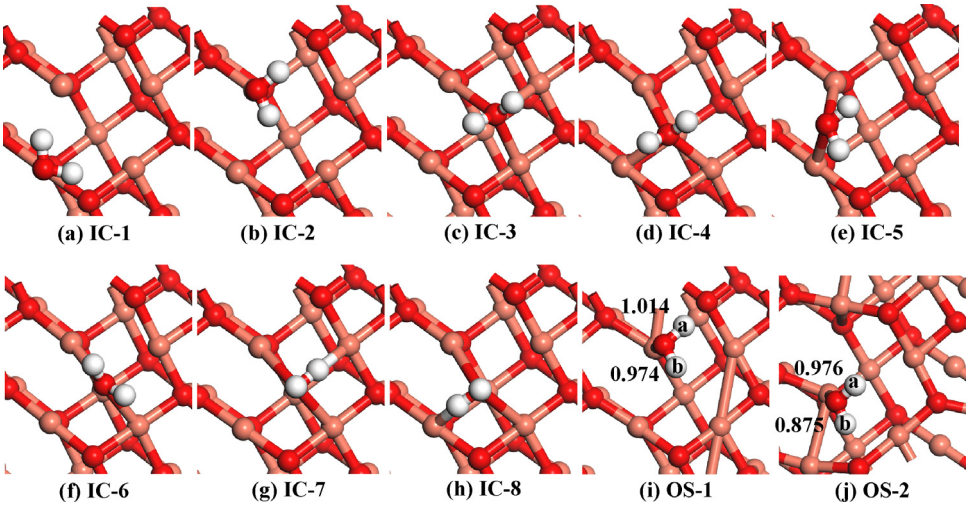

Fig. 5. All possible initial configurations (ICs) and the corresponding optimized structures (OSs) of H_2O adsorbed on the oxygen-vacancy CuO(111) surface. Bond lengths are in Å. See Figs. 1 and 2 for color coding.

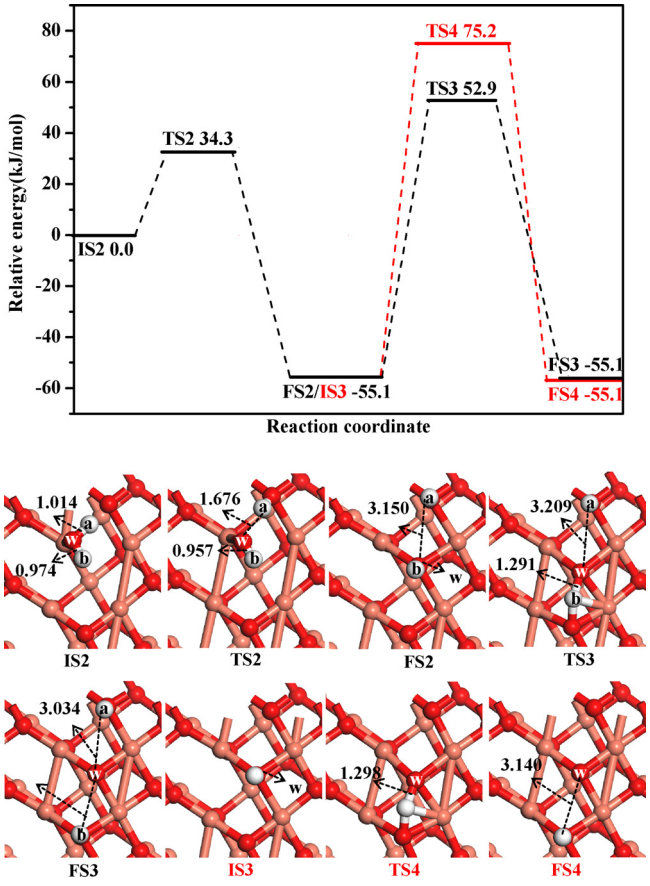

Fig. 6. Potential energy profiles for the dehydrogenation of chemisorption H_2O at Cu^2 site on the oxygen-vacancy surface leading to the final products O and H species adsorbed at $O_{vacancy}$ and O_{SUF} sites, respectively (black line), as well as the dehydrogenation of single OH adsorbed at $O_{vacancy}$ site (red line) together with the initial states (ISs), transition states (TSs) and final states (FSs). Bond lengths are in Å. See Figs. 1 and 2 for color coding. (For interpretation of the references to color in this figure legend, the reader is referred to the web version of the article.)

length of 1.014 Å, subsequently, the first dehydrogenation process ($H_2O_{(ads)} \rightarrow H_{(ads)} + OH_{(ads)}$) occurs, which leads to the formation of O_wH_b group filling the $O_{vacancy}$ site, while the H_a atom is attached to the adjacent O_{SUF} site. The stretch of O_w—H_a bond is the dominating reaction in this step, this bond length is extended to 1.676 Å in TS2, 3.150 Å in FS2 from 1.014 Å in IS2. The activation barrier and reaction energy of this elementary step are 34.3 and −55.1 kJ mol^{-1}, respectively.

3.4.3. OH dissociation

For OH dissociation on the oxygen-vacancy surface, since the previous study by Zhang et al. [62] reported that the presence of H atom (produced from H_2S dissociation) on the stoichiometric $Cu_2O(111)$ surface is in favor of the HS dissociation relative to the dissociation step of single SH group, we still consider the effect of the neighboring H atom (produced from the first step dissociation of chemisorption H_2O) on OH dissociation.

3.4.3.1. OH from chemisorption H_2O. Aiming at studying the effect of the neighboring H atom on OH dissociation, we choose FS2 as the initial state of OH dissociation, as presented in Fig. 6.

Starting from FS2, along with the elongation of O_w—H_b bond length, the O_w—H_b bond gradually cleavages, namely, H_b atom is removed from the O_wH_b fragment leading to FS3 configuration, in which both H_a and H_b are all bonded to the O_{SUF} site, while O_w is adsorbed at the $O_{vacancy}$ site. This reaction via the transition state TS3 requires to overcome an activation barrier of 108.0 kJ mol^{-1}, which is almost thermal neutral (<0.1 kJ mol^{-1}). In TS3, the activated O_w—H_b bond is elongated to 1.291 Å, which is longer than that in FS2 (0.975 Å), and the length of O_w—H_b bond is 3.019 Å in FS3.

3.4.3.2. OH of single adsorption. As already presented in Fig. 2(j), single OH group with O-down mode adsorbed at the $O_{vacancy}$ site is the most favorable configuration on the oxygen-vacancy surface, which is selected as the initial state (IS3) in order to gain a deep knowledge of the H—O bond-breaking process and the diffusion of hydrogen atom on the surface. Beginning with IS3, O_wH breaks its O_w—H bond and directly forms FS4 via TS4, in TS4, the H atom of O_wH group bonds to an adjacent O_{SUF}–Cu_{SUF} bridge site, in which the activated O_w—H bond is elongated to 1.298 Å from 0.976 Å in IS3. In FS4, H is adsorbed at the O_{SUF} site, O_w atom still fills the $O_{vacancy}$ site, this elementary reaction has a high activation barrier of 130.3 kJ mol^{-1}, which is also thermal neutral (<0.1 kJ mol^{-1}), suggesting that the dissociation of single OH group is difficult to occur on the oxygen-vacancy surface.

Table 2
Selected geometrical parameters and Mulliken charge for the adsorbates of the single OH and the co-adsorbed OH + H on different CuO(111) surfaces.

Parameters and charge	Oxygen-vacancy		Oxygen-rich	
	OH (IS3)	OH + H (FS2)	OH (IS5)	OH + H (FS5)
$d_{O\text{-}H}$ (Å)[a]	0.976	0.975	0.980	0.979
$d_{H\text{-}X}$ (Å)[b]	3.169	2.972	3.970	2.981
Charge of H (e)	0.300	0.290 (OH) 0.289 (H)	0.307	0.301 (OH) 0.303 (H)
Charge of O (e)	−0.505	−0.507	−0.454	−0.459
Charge of OH (e)	−0.205	−0.217	−0.147	−0.158

[a] $d_{O\text{-}H}$ (Å) is the O—H bond length.
[b] $d_{H\text{-}X}$ (Å) is the distance between H atom and its adsorption site after O—H bond dissociation.

3.4.4. Brief summary

For the adsorption and dissociation of H_2O on the oxygen-vacancy surface, H_2O adsorbed at the Cu^2 site with O-down mode is the most stable configuration, which dominantly contributes to the formation of OH and H species from H_2O dissociation. As presented in Fig. 6, since OH dissociation has a higher activation barrier relative to the first dehydrogenation reaction of H_2O, the dehydrogenation step of OH from chemisorption H_2O in the presence of neighboring H is difficult to dissociate into the final products H and O atoms compared to the first dehydrogenation step of H_2O leading to OH species. On the other hand, our results also indicate that the single OH species with the absence of neighboring H atom (IS3) occurs at a higher activation barrier (130.3 kJ mol^{-1}) compared to that (108.0 kJ mol^{-1}) of OH with the presence of neighboring H atom from chemisorption H_2O (FS2). Comparing the structures of IS3 and FS2, we can obtained from Table 2 that the O—H bond length of OH (0.976 Å) in IS3 is almost same with that (0.975 Å) in FS2, however, the distance between H atom from OH and its adsorption site after O—H bond dissociation (the adjacent O_{SUF} site) is elongated to 3.169 Å in IS3 from 2.972 Å in FS2, which means that the shorter the distance is, the easier the OH activation is. Meanwhile, OH charges are −0.205 e in IS3 and −0.217 e in FS2, respectively, suggesting that the more the obtained charge of OH is, the easier the OH activation is. The results obtained by charge distributions and inter-atomic distances agree well with that by activation barrier of OH dissociation. As a result, the presence of H atom (produced from the initial step of H_2O dissociation) can promote OH dissociation, OH and H species are still energetically the most favorable products on the oxygen-vacancy surface, which is consistent with the results on the stoichiometric surface.

3.5. Adsorption and dissociation of H_2O on the oxygen-rich surface

As mentioned above, since OH species is the main product of H_2O dissociation on CuO(111) surface, OH species may interact each other by OH + OH combination pathway, which contribute to the formation of surface oxygen-rich atoms on CuO(111) surface. Thus, we further explore the role of the oxygen-rich atom on the surface in the adsorption and dissociation of H_2O. Since atomic O prefers to adsorb at the Cu_{SUB}–Cu_{SUB} bridge site, the structure shown in Fig. 7(a) is employed to model the oxygen-rich CuO(111) surface, in which the atomic O_p is located at the Cu_{SUB}–Cu_{SUB} bridge site.

3.5.1. Atomic O and H adsorption

The structures O(Cu_{SUB}–Cu_{SUB}) and O(Cu_{SUB}), as shown in Figs. 7(b) and (c), represent two stable adsorption configurations of O atom on the oxygen-rich CuO(111) surface, which have the corresponding adsorption energies of 307.8 and 202.9 kJ mol^{-1}, respectively, suggesting that the Cu_{SUB}–Cu_{SUB} bridge site is the most stable adsorption site for atomic O on the oxygen-rich surface.

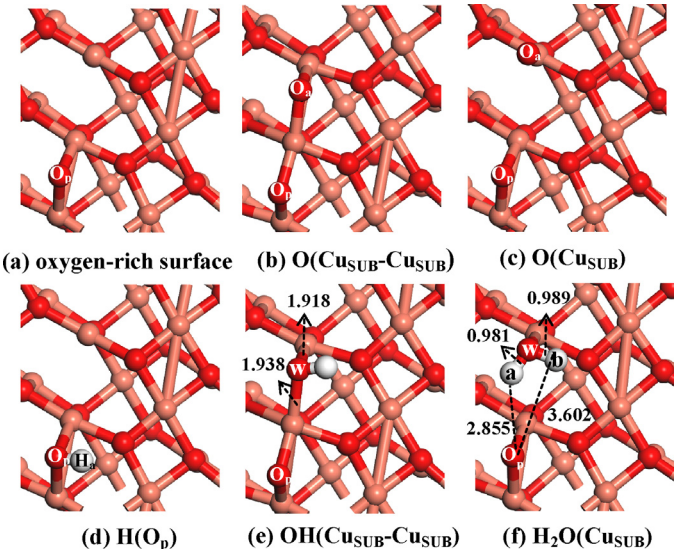

Fig. 7. The side view of oxygen-rich surface, and the optimized stable adsorption configurations of O, H, OH and H_2O species on the oxygen-rich surface. Bond lengths are in Å. See Figs. 1 and 2 for color coding.

Since H adsorbed at the O_{SUF} site is the most stable adsorption configuration on the stoichiometric surface, on the oxygen-rich surface, we also consider atomic H adsorption at the O_p site except for O_{SUF} site, the corresponding adsorption energy is 456.6 kJ mol^{-1}, which is significantly higher than that at the O_{SUF} site (343.9 kJ mol^{-1}), suggesting that O_p site is the most favorable adsorption site for H on the oxygen-rich surface, the optimized stable configuration is presented in Fig. 7(d).

3.5.2. OH adsorption

For OH adsorption, O-down and H-down at the different sites are considered on the oxygen-rich surface. Our results show that OH with O-down adsorbed at the Cu_{SUB}–Cu_{SUB} bridge site is the most stable configuration, as presented in Fig. 7(e), which is similar with that on the stoichiometric surface. In this structure, two Cu—O bonds (1.938 and 1.918 Å) are formed; the corresponding adsorption energy is 272.5 kJ mol^{-1}. Meanwhile, our calculated bands at 3629 and 890 cm^{-1} are attributable to the O—H stretching and Cu—O—H bending modes of adsorbed OH species, respectively.

3.5.3. H_2O adsorption

For H_2O adsorption, the different sites on the oxygen-rich surface have been considered, two types of initial configurations are tested: (1) H_2O is perpendicular to the surface with O binding to the adsorption sites. (2) H_2O is parallel to the surface with O binding to the adsorption sites. After optimization, H_2O parallel to the surface with O binding to Cu_{SUB} site is the only stable configuration, as shown in Fig. 7(f), the adsorption energy is 93.1 kJ mol^{-1}, which is larger than that on the stoichiometric surface (87.0 kJ mol^{-1}). As listed in Table 3, due to the effect of oxygen-rich atom, some properties on the stoichiometric surface will change as follows: firstly, the distance between O_w and nearby Cu atom is shortened by 0.017 Å; secondly, the charge of H_2O is 0.189 and 0.208 e on the stoichiometric and oxygen-rich surface, respectively; these results suggest that the oxygen-rich atom enhances the adsorption strength of H_2O on CuO(111) surface. Further, since the mutual distance between H_a atom of H_2O and O_p atom (2.855 Å) on the oxygen-rich surface is longer than that for H_a and O_{SUF} atom on the stoichiometric surface (1.856 Å), the O_w—H_a bond of H_2O (0.981 Å) on the oxygen-rich

Table 3
Mulliken charge of the adsorbed H_2O on different CuO(111) surfaces.

Parameters and charge	Stoichiometric H_2O	Oxygen-vacancy H_2O	Oxygen-rich H_2O+O_p
$d_{O\text{-}Cu}$ (Å)	2.124	2.026	2.107
Charge of H (e)	0.324	0.345	0.311
	0.294	0.276	0.313
Charge of O (e)	−0.429	−0.427	−0.416 (H_2O)
			−0.437 (O_p)
Charge of H_2O (e)	0.189	0.194	0.208

surface is shorter than that on the stoichiometric surface (0.998 Å). Moreover, the O_w—H_a bond of H_2O (0.981 Å) is longer than that in the free H_2O molecule (0.970 Å), which can contribute to the O—H bond activation of chemisorption H_2O. The bands for adsorbed H_2O appear at 3642 and 3454 cm^{-1} correspond to the O_w—H_a and O_w—H_b bond stretching vibrations, respectively, and 1600 cm^{-1} is contributed to the H—O—H bending mode. As a result, the stable configuration of H_2O parallel to the surface with O binding to the Cu_{SUB} site is chosen as the initial state (IS4) for our investigation about H_2O adsorption and dissociation on the oxygen-rich surface.

3.5.4. H_2O dissociation

Beginning with IS4, the O_w—H_a bond dissociation is considered, the O_w—H_a bond cleavage can form the co-adsorbed OH and H species (FS5) via a transition state (TS5), the corresponding activation barrier is 27.9 kJ mol^{-1}, and this elementary reaction is found to be strongly exothermic by 77.3 kJ mol^{-1}. In TS5, the dissociating O_w—H_a bond distance is 1.183 Å, the O_p—H_a bond length is 1.307 Å. In FS5, H_a atom is transferred to the O_p atom to form two hydroxyls of O_wH_b and O_pH_a adsorbed at two adjacent Cu_{SUB}–Cu_{SUB} bridge sites via oxygen atom, respectively.

3.5.5. OH dissociation

3.5.5.1. OH from chemisorption H_2O. The O—H bond cleavage of O_wH_b is considered in this section. Starting from FS5, the final product (FS6) can be formed via a transition state TS6 with the H_b atom migrates from O_w atom to surface O_{SUF} atom. In TS6, the H_b—O_w bond is elongated from 0.979 Å in FS5 to 1.268 Å, and finally elongated to 3.253 Å in FS6. This elementary reaction is highly endothermic by 80.1 kJ mol^{-1} with a significantly large activation barrier of 145.8 kJ mol^{-1}.

3.5.5.2. OH of single adsorption. As already presented in Fig. 7(e), the single OH group adsorbed at the Cu_{SUB}–Cu_{SUB} bridge site is selected as the initial state (IS5). We can see from Fig. 8 that IS5 goes through TS7 to form FS7, in TS7, the H atom of O_wH group moves toward the Cu_{SUB} site, where the activated O_w—H bond is elongated to 2.000 Å from 0.980 Å in IS5. In FS7, H is located at the O_p site, O_w atom is adsorbed at the Cu_{SUB}–Cu_{SUB} bridge site. This elementary reaction has a significantly high activation barrier of 312.1 kJ mol^{-1}, it is slightly exothermic by 2.2 kJ mol^{-1}. Above results mean that the O_w—H bond cleavage of the single OH group on the oxygen-rich surface is difficult to occur in the view of kinetics, this conclusion obtained is consistent with that on the oxygen-vacancy surface.

3.5.6. Brief summary

As shown in Fig. 8, since the dissociation of OH needs to overcome a significantly high barrier relative to the first dehydrogenation step of H_2O, we clearly conclude that OH and H species is the most favorable products. As listed in Table 2, in the absence of neighboring H atom (IS5), the distance between H of the single OH species and its corresponding adsorption site after O—H bond dissociation is elongated to 3.970 Å in IS5 from 2.981 Å in FS5, Meanwhile, OH charges are −0.147 e in IS5 and −0.158 e in FS5, respectively. Similar to oxygen-vacancy surface, the charge

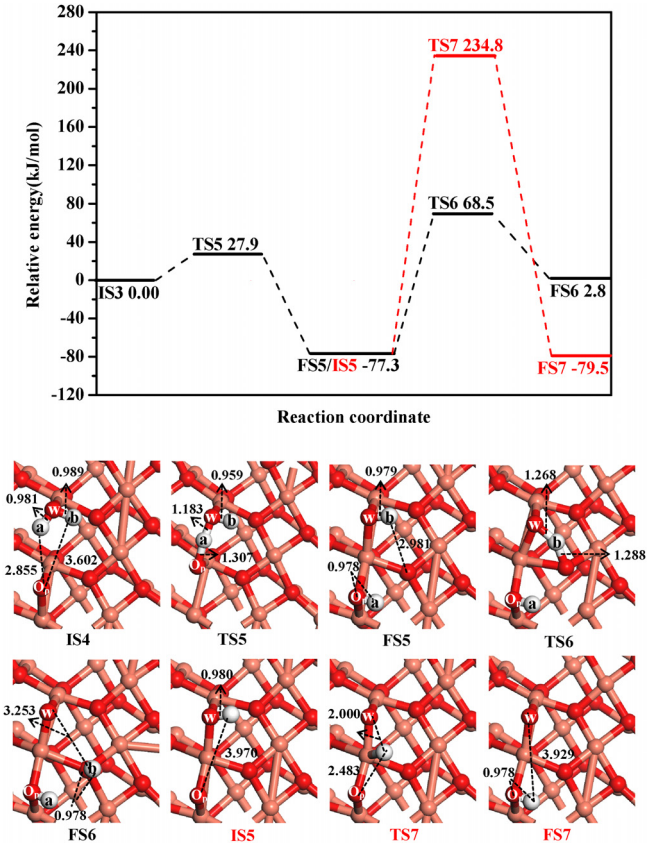

Fig. 8. Potential energy profiles for the dehydrogenation of chemisorption H_2O at Cu_{SUB} site on the oxygen-rich surface leading to the final products O and H species (black line), as well as the dehydrogenation of single OH adsorbed at Cu_{SUB}–Cu_{SUB} bridge site (red line) together with the initial states (IS), transition states (IS) and final states (FS). Bond lengths are in Å. See Figs. 1 and 2 for color coding. (For interpretation of the references to color in this figure legend, the reader is referred to the web version of the article.)

distributions and inter-atomic distances is consistent with the activation barrier of OH dissociation, the presence of H atom (produced from H_2O dissociation) can still promote the OH dissociation on the oxygen-rich surface.

3.6. General discussion

For adsorption and dissociation of H_2O on three types of CuO(111) surfaces, we can clearly find that on the stoichiometric surface, H and O species cannot be formed by OH species dissociation. For the dissociation of the single OH group on the oxygen-vacancy and oxygen-rich surfaces, it occurs at a higher dehydrogenation barrier (Figs. 6 and 8), lower amounts of charge transfer, as well as the longer distance between H atom of OH group and its adsorption site after O—H bond dissociation compared to OH dissociation with the presence of H from H_2O dissociation (see Table 2), suggesting that the presence of H atom (produced from H_2O dissociation) is in favor of OH dissociation. However, our results show that OH dissociation presents a significantly higher barrier than the first dehydrogenation reaction of H_2O leading to OH species, which means that OH species is the dominant product of H_2O dissociation on these three CuO(111) surfaces.

The simplified potential energy diagram for the initial O—H cleavage of chemisorption H_2O leading to dominant OH species is presented in Fig. 9. According to this figure, taking thermodynamics into consideration, the formation of OH species on the stoichiometric surface is endothermic by 30.5 kJ mol^{-1}. In contrast, the dissociation reactions on the oxygen-vacancy and oxygen-rich

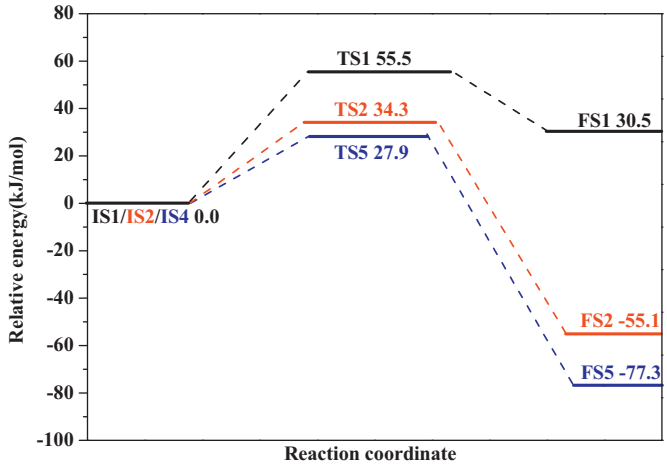

Fig. 9. Schematic potential energy diagrams for the initial O—H bond cleavage of chemisorption H_2O leading to dominant OH species on the stoichiometric surface (black line), the oxygen-vacancy surface (red line), and the oxygen-rich surface (blue line), respectively. (For interpretation of the references to color in this figure legend, the reader is referred to the web version of the article.)

Table 4
The calculated results for gaseous and adsorbed H_2O: antisymmetric stretching frequency (υ_{asym}), symmetric stretching frequency (υ_{sym}), H—O—H bending frequency (υ_{bend}), together with those for gaseous and adsorbed OH group: stretching frequency (υ_{asym}), Cu—O—H bending frequency (υ_{bend}).

	Species	Vibrational frequencies/cm^{-1}		
		υ_{asym}	υ_{sym}	υ_{bend}
H_2O	Stoichiometric	3636	3232	1640
	Oxygen-vacancy	3718	2944	1576
	Oxygen-rich	3642	3454	1600
	Gaseous	3854	3735	1629
OH	Stoichiometric	3661		786
	Oxygen-vacancy	3677		819
	Oxygen-rich	3629		890
	Gaseous	3639		

surfaces are exothermic by 55.1 and 77.3 kJ mol^{-1}, respectively. On the other hand, in the view of kinetics, the dissociation barrier of the initial O—H bond cleavage on the stoichiometric surface and oxygen-vacancy surfaces are 55.5 and 34.3 kJ mol^{-1} respectively. However, on the oxygen-rich surface, this reaction has the lowest barrier (27.9 kJ mol^{-1}) of the initial O—H bond dissociation compared to that on the stoichiometric and oxygen-vacancy surfaces, indicating that the O—H bond cleavage of chemisorption H_2O on the oxygen-rich surface leading to OH species is likely to be the most favorable pathway compared to that on the stoichiometric and oxygen-vacancy surfaces. On the other hand, as presented in Table 3, Mulliken population analysis indicates that the values of charge transfer for H_2O molecule on the oxygen-rich surface is the largest (0.208 e), while that on the stoichiometric surface is lowest (0.189 e), suggesting that the larger the charge transfer is, the stronger the activation of H_2O is, namely, the larger the charge transfer is in favor of H_2O dissociation, which is in line with the results obtained by the activation barrier of H_2O dissociation on these three surfaces. Thus, the oxygen-rich CuO(111) surface is more favorable for the dissociation of chemisorption H_2O leading to OH species than the stoichiometric and oxygen-vacancy surfaces both thermodynamically and kinetically, in which the oxygen-rich atom can act as a promoter.

On the other hand, the vibrational frequencies of the adsorbed H_2O and OH species on these CuO(111) surfaces, as listed in Table 4, suggest that the anti-symmetric and symmetric O—H stretching frequencies of H_2O significantly decrease upon adsorption. Interestingly, the O—H stretching frequency of adsorbed OH is approximately constant upon adsorption. All these data are significant for the experimental study. However, to the best of our knowledge, few experimental results about the vibrational frequencies of H_2O adsorption and dissociation on CuO(111) surfaces have been reported till now. We sincerely hope that more systematically experiments can be performed in the next work, which can be compared with our calculated vibration frequencies to determine the active center of H_2O adsorption and its principal products. In addition, previous experimental studies about the mechanism and kinetics for the oxidative carbonylation of methanol over CuO catalyst have been concerned, in which H_2O acts as a product [30,31], our results may provide a theoretical reference for the effect of H_2O on catalyst surface structure and the dominant existence form of H_2O in the reactions related to H_2O as reactant, product and solvent environment, and so on, under the realistic experiment condition.

4. Conclusions

The adsorption and dissociation of H_2O on the stoichiometric, oxygen-vacancy and oxygen-rich CuO (111) surfaces have been explored using density functional theory calculations, the most favorable configurations and adsorption energies for H_2O, OH, O and H species are obtained. The results show that Cu_{SUB} is the favorable adsorption site of molecular H_2O on the stoichiometric and oxygen-rich surfaces, while Cu^2 is the stable adsorption site on the oxygen-vacancy surface. OH group and O atom adsorbed at the Cu_{SUB}–Cu_{SUB} bridge site are the most stable configurations on the stoichiometric and oxygen-rich surfaces; in the case of oxygen-vacancy surface, $O_{vacancy}$ site is filled with atomic O. H atom is preferentially adsorbed at O_{SUF} site on the stoichiometric and oxygen-vacancy surfaces, while O_p is the favorable adsorption site on the oxygen-rich surface. PDOS results show that H_2O, OH and O atom are adsorbed on the CuO(111) surface by the interaction between *p* orbital of O atoms and *d* orbital of Cu, and the adsorbate–substrate interaction is strongly localized on the surface.

The activation barrier and thermochemistry for the dissociation of H_2O, as well as the single OH group leading to O and H species firstly show that OH species fail to split into H and O on the stoichiometric surface; the dissociation of the single OH group on the oxygen-vacancy and oxygen-rich surfaces has a higher barrier relative to the dehydrogenation barrier of OH from chemisorption H_2O, suggesting that the presence of H atom (produced from H_2O dissociation) can promote OH dissociation. Moreover, the dissociation of OH from H_2O dehydrogenation presents a significantly higher barrier compared to the first dehydrogenation reaction of H_2O leading to OH species, indicating that OH species is the main product of H_2O dissociation on these surfaces. Further, the dissociation barrier of H_2O on the oxygen-vacancy surface is smaller than that on the stoichiometric surface, which means that the oxygen-vacancy can exhibit a strong catalytic activity toward H_2O dissociation into OH and H species. More importantly, the oxygen-rich atom acts as a promoter for the formation of OH species by the first dehydrogenation of H_2O, which is the most favorable both thermodynamically and kinetically than that on other two surfaces. Finally, our calculated vibrational frequencies for the adsorbed H_2O and OH species on different CuO(111) surfaces may play an important role in the experimental research about the surface vibrational spectroscopy.

Acknowledgments

This work is financially supported by the National Natural Science Foundation of China (No. 21276003, 21476155 and 21276171), the Natural Science Foundation of Shanxi Province

(No. 2014011012-2), the Program for the Top Young Academic Leaders of Higher Learning Institutions of Shanxi, and the Top Young Innovative Talents of Shanxi.

References

[1] A.D. Dunnen, M.J.T.C. van der Niet, C. Badan, M.T.M. Koper, L.B.F. Juurlink, Phys. Chem. Chem. Phys. 17 (2015) 8530–8537.
[2] K. Andersson, A. Gómez, C. Glover, D. Nordlund, H. Öström, T. Schiros, O. Takahashi, H. Ogasawara, L.G.M. Pettersson, A. Nilsson, Surf. Sci. 585 (2005) L183–L189.
[3] E.D. German, M. Sheintuch, J. Phys. Chem. C 114 (2010) 3089–3097.
[4] L.Q. Wang, D.R. Baer, M.H. Engelhard, A.N. Shultz, Surf. Sci. 344 (1995) 237–250.
[5] D.L. Doering, T.E. Madey, Surf. Sci. 123 (1982) 305–337.
[6] W.T. Li, S.M. Liu, S. Wang, Q.L. Guo, J.D. Guo, J. Phys. Chem. C 118 (2014) 2469–2474.
[7] D.J. Dai, S.J. Peters, G.E. Ewing, J. Phys. Chem. 99 (1995) 10299–10304.
[8] U. Leist, W. Ranke, K. Al-Shamery, Phys. Chem. Chem. Phys. 5 (2003) 2435–2441.
[9] J.L. Daschbach, Z. Dohnálek, S.R. Liu, R.S. Smith, B.D. Kay, J. Phys. Chem. B 109 (2005) 10362–10370.
[10] C.S. Chen, C.C. Chen, T.W. Lai, J.H. Wu, C.H. Chen, J.F. Lee, J. Phys. Chem. C 115 (2011) 12891–12900.
[11] W.J. Wang, G.P. Wang, J. Energy Inst. 88 (2015) 112–117.
[12] S. Yamamoto, A. Beniya, K. Mukai, Y. Yamashita, J. Yoshinobu, J. Phys. Chem. B 109 (2005) 5816–5823.
[13] R.Q. Liu, Comput. Theor. Chem. 1019 (2013) 141–145.
[14] M. Klaua, T.E. Madey, Surf. Sci. 136 (1984) 42–50.
[15] Y.L. Cao, Z.X. Chen, Phys. Chem. Chem. Phys. 9 (2007) 739–746.
[16] G.C. Wang, S.X. Tao, X.H. Bu, J. Catal. 244 (2006) 10–16.
[17] G.R. Sheffer, T.S. King, J. Catal. 115 (1989) 376–387.
[18] R.G. Herman, K. Klier, G.W. Simmons, B.P. Finn, J.B. Bulko, T.P. Kobylinski, J. Catal. 56 (1979) 407–429.
[19] G.C. Chinchen, P.J. Denny, J.R. Jennings, M.S. Spencer, K.C. Waugh, Appl. Catal. 36 (1988) 1–65.
[20] Y. Kanai, T. Watanabe, T. Fujitani, T. Uchijima, J. Nakamura, Catal. Lett. 38 (1996) 157–163.
[21] Z.J. Zuo, W. Huang, P.D. Han, Z.H. Li, Appl. Surf. Sci. 256 (2010) 2357–2362.
[22] N.D. McClenaghan, P.J. Hu, C. Hardacre, Surf. Sci. 464 (2000) 223–232.
[23] R.G. Zhang, B.J. Wang, L.X. Ling, H.Y. Liu, W. Huang, Appl. Surf. Sci. 257 (2010) 1175–1180.
[24] R.G. Zhang, H.Y. Liu, H.Y. Zheng, L.X. Ling, Z. Li, B.J. Wang, Appl. Surf. Sci. 257 (2011) 4787–4794.
[25] S.A. Saraireh, M. Altarawneh, Can. J. Phys. 91 (2013) 1101–1106.
[26] R.G. Zhang, J.R. Li, B.J. Wang, L.X. Ling, Appl. Surf. Sci. 279 (2013) 260–271.
[27] Y. Li, L.F. Yan, G.C. Wang, J. Nat. Gas Chem. 20 (2011) 155–161.
[28] M. Li, J.Y. Zhang, Y. Zhang, G.F. Zhang, T.M. Wang, Appl. Surf. Sci. 257 (2011) 10710–10714.
[29] R.G. Zhang, H.Y. Liu, L.X. Ling, Z. Li, B.J. Wang, Appl. Surf. Sci. 257 (2011) 4232–4238.
[30] Y.J. Wang, R.X. Jiang, X.Q. Zhao, S.F. Wang, J. Nat. Gas Chem. 9 (2000) 205–212.
[31] H.T. Zhang, S.F. Wang, X.Q. Zhao, Y.J. Wang, J. Hebei Univ. Technol. 33 (2004) 36–40.
[32] H.T. Hsueh, S.J. Chang, F.Y. Hung, W.Y. Weng, C.L. Hsu, T.J. Hsueh, S.S. Lin, B.T. Daic, J. Electrochem. Soc. 158 (2011) J106–J109.
[33] J. Hu, D.D. Li, J.G. Lu, R.Q. Wu, J. Phys. Chem. C 114 (2010) 17120–17126.
[34] X. Hu, J. Schuster, S.E. Schulz, T. Gessner, Phys. Chem. Chem. Phys. 17 (2015) 26892–26902.
[35] Y. Maimaiti, M. Nolan, S.D. Elliott, Phys. Chem. Chem. Phys. 16 (2014) 3036–3046.
[36] S. Yin, X.Y. Ma, D.E. Ellis, Surf. Sci. 601 (2007) 2426–2437.
[37] S.J. Sun, C.Y. Li, D.S. Zhang, Y.J. Wang, Appl. Surf. Sci. 333 (2015) 229–234.
[38] W.K. Chen, S.H. Liu, M.J. Cao, Q.G. Yan, C.H. Lu, J. Mol. Struct.: THEOCHEM 770 (2006) 87–91.
[39] V. Efstathiou, D.P. Woodruff, Surf. Sci. 526 (2003) 19–32.
[40] R.B. Barros, A.R. Garcia, L.M. Ilharco, J. Phys. Chem. B 108 (2004) 4831–4839.
[41] Q. Sun, Y. Wang, K.N. Fan, J.F. Deng, Surf. Sci. 459 (2000) 213–222.
[42] B.R. Shen, Z.G. Fang, K.N. Fan, J.F. Deng, Surf. Sci. 459 (2000) 206–212.
[43] X. Wang, W.K. Chen, C.H. Lu, Appl. Surf. Sci. 254 (2008) 4421–4431.
[44] S.J. Sun, Y.J. Wang, Q.S. Yang, Appl. Surf. Sci. 313 (2014) 777–783.
[45] A. Filippetti, V. Fiorentini, Phys. Rev. Lett. 95 (2005) 086405.
[46] W.J. Xiang, J. Liu, M. Chang, C.G. Zheng, Chem. Eng. J. 200–202 (2012) 91–96.
[47] S.J. Sun, D.S. Zhang, C.Y. Li, Y.J. Wang, RSC Adv. 5 (2015) 21806–21811.
[48] B. Delley, J. Chem. Phys. 92 (1990) 508–517.
[49] B. Delley, J. Chem. Phys. 113 (2000) 7756–7764.
[50] J.P. Perdew, K. Burke, M. Ernzerhof, Phys. Rev. Lett. 77 (1996) 3865–3868.
[51] P. Hu, D.A. King, S. Crampin, M.H. Lee, M.C. Payne, Chem. Phys. Lett. 230 (1994) 501–506.
[52] J.P. Perdew, Y. Wang, Phys. Rev. B: Condens. Matter 45 (1992) 13244–13249.
[53] P. Hohenberg, W. Kohn, Phys. Rev. 136 (1964) B864–B871.
[54] Y. Inada, H. Orita, J. Comput. Chem. 29 (2008) 225–232.
[55] T.A. Halgren, W.N. Lipscomb, Chem. Phys. Lett. 49 (1977) 225–232.
[56] A.D. Fortes, J.P. Brodholt, I.G. Wood, L. Vočadlo, H.D.B. Jenkins, J. Chem. Phys. 115 (2001) 7006–7014.
[57] S. Asbrink, L.J. Norrby, Acta Crystallogr. B 26 (1970) 8–15.
[58] R. Liu, W. Shen, J. Zhang, M. Li, Appl. Surf. Sci. 254 (2008) 5706–5710.
[59] Y.C. Huang, Z.X. Chen, J. Phys. Chem. C 115 (2011) 18752–18760.
[60] R.T. Vang, K. Honkala, S. Dahl, E.K. Vestergaard, J. Schnadt, E. Laegsgaard, B.S. Clausen, J.K. Norskov, F. Besenbacher, Nat. Mater. 4 (2005) 160–162.
[61] B.L.M. Hendriksen, M.D. Ackermann, R. van Rijn, D. Stoltz, I. Popa, O. Balmes, A. Resta, D. Wermeille, R. Felici, S. Ferrer, J.W.M. Frenken, Nat. Chem. 2 (2010) 730–734.
[62] R.G. Zhang, H.Y. Liu, J.R. Li, L.X. Ling, B.J. Wang, Appl. Surf. Sci. 258 (2012) 9932–9943.